Impact of the Geometric Scaling on the Desing of Sub-THz Frequency-Selective Surface

G. Hilario-Perez [1], P. Córdova-Morales [1], A. D. Morales-Vite [1], E. Lugo-Hernández [2], D. Valdez-Perez [1], J.D. García-Aguilar [4], Angel A. Duran-Ledezma [3]
[1]Instituto Politécnico Nacional, SEPI-ESIME-Zac, UPALM, Edif. Z-4 3er Piso, CP 07738, CDMX, México.
[2]Universitat Politécnica de Catalunya, Departamento de Teoría de la Señal y Comunicaciones, Barcelona, España
[3] SEPI, ESIME Ticomán, Instituto Politécnico Nacional, Av. Ticomán No. 600, San José Ticomán, 07340, México City, México.
[4]Instituto Politécnico Nacional, Centro de Estudios Científicos y Tecnológicos N° 16 "Hidalgo", Kilómetro 1.500, Actopan - Pachuca, San Agustín Tlaxiaca, Hgo.
ghilariop1300@alumno.ipn.mx, amoralesv1704@alumno.ipn.mx, pcordovam1800@alumno.ipn.mx, eduardo.telematica@upc.edu, dvaldez@ipn.mx, aduran@ipn.mx.
URL ORCID: https://orcid.org/0009-0007-7058-2201

Abstract

In this work, we analyzed the effects of varying the size of the shapes that compose a Sub-THz frequency-selective surface (FSS) to study the impact of inter-element spacing. We designed and simulated a unit cell with ring-shaped elements using finite element software. The results demonstrated a significant redshift (displacement toward lower frequencies) when the shapes are positioned closer together, in contrast to the shift toward higher frequencies observed at greater separations. Consequently, we concluded that the resonance frequency shifts by 1.05 GHz when the geometry increases by 0.0025 mm², and approximately doubles the frequency displacement when the area increases to 0.005 mm². This result indicates that doubling the unit of the geometry's area causes the resonance frequency to shift by twice as much as well.

Keywords **— Frequency selective surface (FSS), Sub-THz, 6G wireless communications, Passive filters.**

I. INTRODUCTION

Frequency selective surfaces (FSSs) and emerging technologies, such as metasurfaces[1], [2], [3], metamaterials [4], [5], [6], [7], and 2D materials like graphene and the novel MXenes, have attracted significant attention in the scientific community in recent decades due to their impressive mechanical, electrical, thermal, and optical properties[8], [9], [10], [11], [12], as well as their ability to control electromagnetic waves, as is the case with metasurfaces and FSSs. These technologies' development represents a significant advancement in creating compact micro- and nano-scale components and devices that can be integrated into optoelectronic and photonic systems, which are essential for applications in various fields such as security, medicine, and especially telecommunications.[13], [14], [15], [16], [17]. The study of the FSSs began with a documented scientific exchange between Francis Hopkinson and the American physicist David Rittenhouse, published in 1786. Hopkinson described a curious phenomenon involving a silk handkerchief, stating: “Agreeably to my expectation I observed the filk threads magnified to the size of very coarse wires; but was much surprised to find that, although I moved the handkerchief to the right and left before my eyes, the dark bars did not seem to move at all, but remained permanent before the eye.” [18] This observation motivated the study of periodic structures, and it is reported that the first patent related to FSSs was filed in 1919 by Marconi and Franklin, who designed a parabolic reflector consisting of a non-continuous surface made of horizontal wires. Later, FSSs began to attract intensive research interest for military applications around the mid-20th century.[19], [20], [21], [22], [23]. Over time, with an increased understanding of this technology and the development of other technologies, new applications emerged (see Figure 1).

FSSs, like metasurfaces and metamaterials, are based on periodic patterns (see Figure 2). This technology consists of a matrix of elements referred to as unit cells, which are analogous to the atoms of a material. These unit cells define the periodicity of the structure and the properties that characterize it [22], [24].

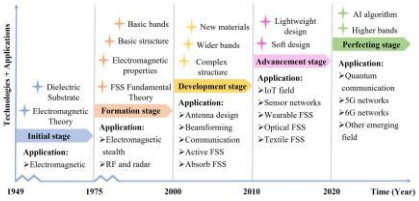

Figure 1.- Representation of development road map for FSSs.[25]

The behavior and performance of FSSs depend significantly on the geometry of their resonator elements. Over the past few decades, numerous geometries have been studied and classified into different categories, as shown in Figure 3.[22] These studies aim to determine the resonance frequency, bandwidth, and optimal control of electromagnetic fields efficiently, enabling FSSs to selectively transmit or directionally reflect electromagnetic waves across a broad spectrum, ranging from microwaves to optics, including the Terahertz (THz) band gap. [19], [21] Currently, FSSs have garnered extensive attention because they are becoming increasingly crucial for sixth-generation (6G) communication systems (see Figure 2b), as well as for intelligent, reflective surfaces (IRSs), given their

capacity to suppress interference and improve channel quality.[25], [26], [27]

Figure 2.- a) Schematic representation of a Frequency Surface Selective with ring elements. 'S' is the incident wave, 'Sr' is the reflected wave, and 'St' is the transmitted wave. b) Illustration of FSS-assisted future 6G networks.[25]

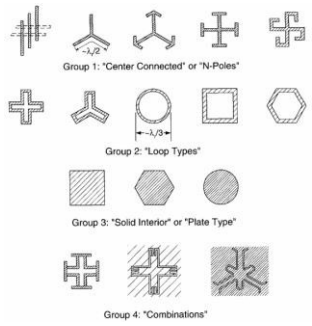

Figure 3.- Different shapes of resonant elements arranged in groups.[22]

In this work, we aim to contribute to the state of the art by analyzing the effects of inter-element spacing and improving the efficiency of frequency-selective surfaces (FSSs) through precise prediction of their behavior. The novelty of this study lies in presenting the relationship between changes in the area of the resonator elements and the displacement in the resonance frequency. We designed a unit cell and calculated its resonance using a simple resonant circuit. Subsequently, we analyzed the structure with different distances of the inter-element spacing using finite element software. Finally, we discuss the results and present our conclusions.

II. STRUCTURE DESIGN AND SIMULATIONS

This work considers a unit cell with loop-type geometry elements, forming a Frequency Selective Surface (FSS). The FSS is modeled using the equivalent circuit shown in Figure 1b, which is only valid for normal incident waves. In this simple resonant circuit, the copper ring represents the inductive part, while the distance between the elements represents the capacitance of the proposed structure (see Figure 4a). This method of design is used to approximately determine the resonance frequency.

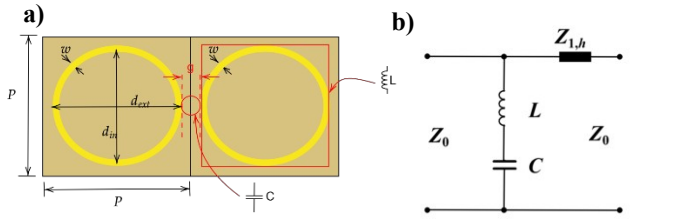

Figure 4.- a) Schematic representation of two unit cells that form an FSS with ring-type elements, where the rings are modeled as the inductive part (L) and the distance between elements as the capacitive part (C).
b) Equivalent circuit of the FSS.

Z_0 is the impedance of free, and Z_{1h} represents the substrate; L and C are the equivalent inductance and capacitance, respectively. To obtain the resonant frequency f, we need to calculate L and C considering the following equations:[27], [28], [29]

$$L = \mu_0 \frac{p}{2\pi} \log\left[sin^{-1}\left(\frac{\pi w}{2p}\right)\right] \quad (1)$$

$$C = \epsilon_0 \epsilon_{eff} \frac{2w}{\pi} \log\left[sin^{-1}\left(\frac{\pi g}{2w}\right)\right] \quad (2)$$

$$\epsilon_{eff} = \frac{\epsilon_r + 1}{2} \quad (3)$$

In this case, "p" is the periodicity of the elements the 1mm, w=0.2mm is the width defined by the inner diameter "d_{in}" and the outer diameter "d_{ext}", g=0.0001mm is the inter-element spacing, ε_r is the relative permittivity of the substrate, ε_{ff} is the effective permittivity of the substrate, ε_0 is the permittivity of free equal to $8.854x\,10^{-12}\ [F/m]$, and μ_0 equal to $4\pi x10^{-7}\ [H/m]$ is the permeability. The resonant frequency can be calculated as

$$f = \frac{1}{2\pi\sqrt{LC}} \quad (4)$$

A computational program was used, which provides various numerical methods for solving problems and conducting electromagnetic analysis, such as the Finite Element Method (FEM). For the material properties used in the design and simulation of the unit cell, copper was assigned an electrical conductivity of 5.8×10^7 S/m. At the same time, Arlon AD 300D was modeled with a relative permittivity of 2.98 and a loss tangent of 0.002.

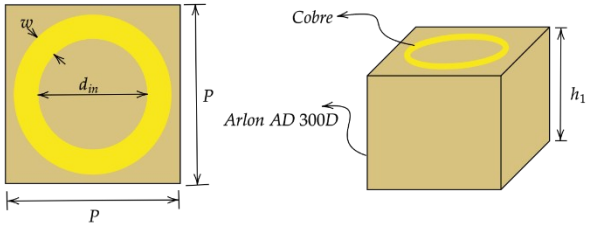

Figure 5.- Representation of the FSS unite-cell, where "P" is the periodicity, "din" is the inner diameter, and "w" is the broad of the ring.

Figure 5 illustrates the unit cell structure, where the ring has an inner radius "din" and an outer radius "dext", which could be modified by maintaining the same ring width of "w" but modifying the value of "g". The dielectric thickness is 0.05 mm, and the resonator thickness is 100 nm. Those geometric parameters, including the ring width, remain constant throughout the study, as shown in Figure 6.

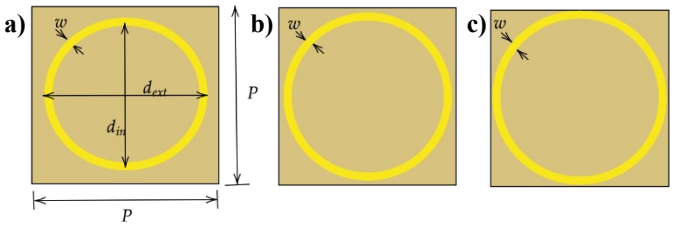

Figure 6. In the figure, we can see a) the element with initial diameters and a defined "w" and b) and c) how the radius is more significant, but "w" has the same value.

The intention is to analyze the behavior when the varied parameters are the internal and external diameters of the ring. The analysis begins with an inner radius of 0.2 mm and an outer radius of 0.4 mm (Figure 6a), incrementing in steps of 0.02 mm until reaching an inner radius of 0.28 mm and an outer radius of 0.48 mm. As a final case, an inner radius of 0.299 mm and an outer radius of 0.499 mm are considered, resulting in a spacing between resonators of 0.001 mm. Figures 6b and 6c show the chances of the resonator element.

III. Results and Discussion

The resonance frequency can be calculated using Equation (4), taking the values from Equations (1) and (2) with p=1mm, g=0.0001mm, and w=0.0002mm. From these calculations, we obtained L=0.252nH, C=0.384pF, and a resonant frequency of 161.15GHz, similar to the resonant frequency obtained from the simulation, as shown in the following graph.

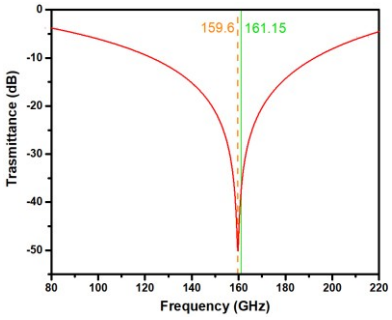

Figure 7. Resonance response under normal incidence: The simulation results are dashed lines, and the calculated by the equivalent circuit analysis is indicated by a solid line.

After analyzing the resonance frequency, we considered different sizes of the elements, adjusting each radius by 0.02mm and, in some cases, by half. The analysis started with an outer radius ranging from 0.4mm to 0.49mm, given that the resonance at 161GHz was achieved with an outer radius of 0.45mm and an inner radius of 0.25mm. As previously mentioned, this involved varying the inter-element spacing by reducing or increasing the radius of the elements.

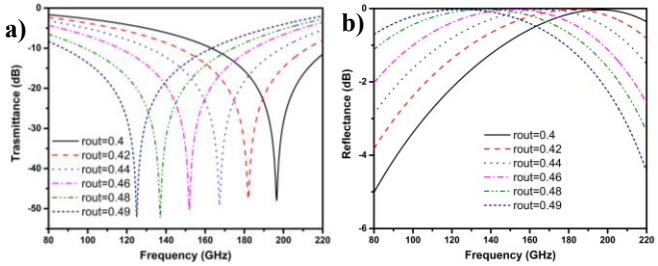

Figure 8. The following graph shows a) the transmittance coefficient and b) the reflectance coefficient.

Figure 8 shows the transmission (see Figure 8a) and reflectance (see Figure 8b). We observe that when the inter-element spacing increases, the resonant frequency shifts toward higher frequencies, and when the spacing decreases, the resonance shifts toward lower frequencies. In Table 1, we can see the values and differences for each change. Notably, from an outer radius of 0.4mm to 4.8mm, each increment of 0.02mm results in a frequency displacement of approximately 14GHz, with one exception highlighted in yellow in Table 1. In this case, the increment was 0.01mm for both diameters, resulting in a displacement of approximately 12GHz, nearly the same displacement observed when the radius is increased by 0.02mm.

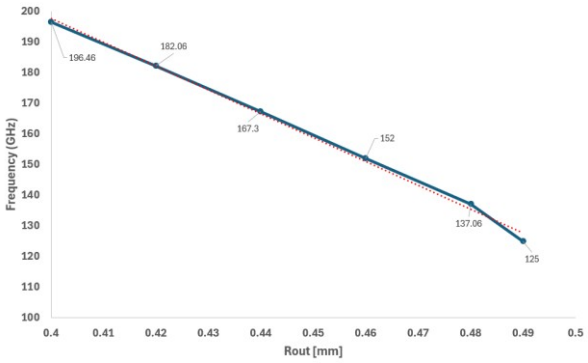

Figure 9.- Tendence of the displacement of the frequency versus the increase of the radius where the dashed line is the trend.

In Figure 9, we can observe that the results indicate an almost linear relationship between the increase in geometry (i.e., the reduction in distance between the elements) and the displacement toward lower frequencies. Based on this, we expected a frequency displacement of approximately half the value observed in the previous case when transitioning from 0.48mm to 0.49mm. It is essential to mention that, as shown in Table 1, when the diameters are increased by 0.02mm, the area of the resonant element changes by 0.05 mm2. Consequently, when the area increases by 0.05mm ^{2}, the displacement in frequency is approximately 14GHz.

Tabla 1.- Results of the case 1

r_{out} [mm]	r_{in} [mm]	w [mm]	f_r [GHz]	S21 [dB]	Δf [GHz]	ΔS21 [dB]	Área [mm^2]	ΔÁrea [mm^2]
0.4	0.2	0.2	196.46	−47.97			0.75	
0.42	0.22	0.2	182.06	−47.63	14.4	−0.34	0.8	0.05
0.44	0.24	0.2	167.3	−49.23	14.76	1.6	0.85	0.05
0.46	0.26	0.2	152	−50.45	15.3	1.22	0.9	0.05
0.48	0.28	0.2	137.06	−52.24	14.94	1.79	0.95	0.05
0.49	0.29	0.2	125	−52.05	12.06	−0.19	0.98	0.025

We investigated whether changes in the resonant area maintain a linear behavior to analyze the behavior better when the elements are very close together (given that the transition from 0.48mm to 0.49mm no longer exhibits a linear response). For this purpose, we analyzed area changes of 0.005mm ^{2} and 0.0025mm ^{2}. In other words, starting from an outer radius of 0.49mm, we increased it to 0.499mm. The results obtained are shown in Table 2. We plot the frequency displacement changes according to the radius variation, as shown in Figure 9.

Table 2.- Results of the case 2

r_{out} [mm]	r_{in} [mm]	w [mm]	f_r [GHz]	S21 [dB]	Δf [GHz]	ΔS21 [dB]	Área [mm^2]	ΔÁrea [mm^2]
0.49	0.29	0.2	125	−52.05			0.981	
0.492	0.292	0.2	123.03	−50.33	1.98	−1.72	0.986	0.005
0.494	0.294	0.2	120.3	−49.23	2.72	2.72	0.991	0.005
0.496	0.296	0.2	152	−50.45	3.3	3.3	0.996	0.005
0.498	0.298	0.2	137.06	−52.24	3.88	3.88	1.0012	0.005
0.499	0.299	0.2	125	−52.05	3.42	−3.42	1.0037	0.0025

In Table 2, we can observe that the frequency displacements are somewhat similar when the area of the elements increases by 0.005mm ^{2}. Additionally, as highlighted in yellow, we see that when the area increases by 0.0025mm ^{2}, the resulting frequency displacement is similar to that observed for an increase of 0.005mm ^{2}. This is consistent with the previous case, where just like in this case we expected the frequency displacement to be half of the observed value.

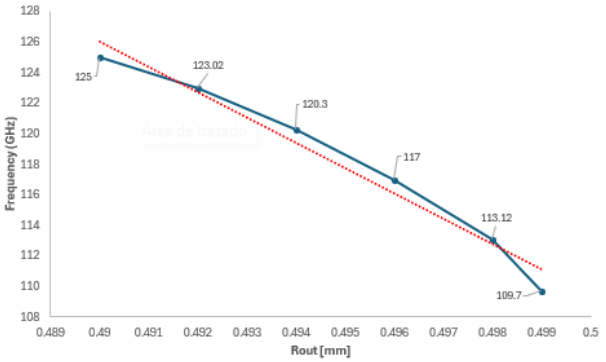

Figure 10.- The trend of frequency displacement as a function of increasing radius is shown, with the dashed line representing the tren d.

With the intention of determining whether this case exhibits linear behavior, we examined the case where the elements are somewhat separated. The results in Table 3 and Figure 11 show improved behavior, indicating that when the area increment is of 0.005mm2 the displacement in frequency is to similar anin this case when the outer radius changes from 0.428mm to 0.429mm, the frequency displacement is approximately half, how we expected and that this did not happen previous cases, where shorter distances between elements did not exhibit such a trend.

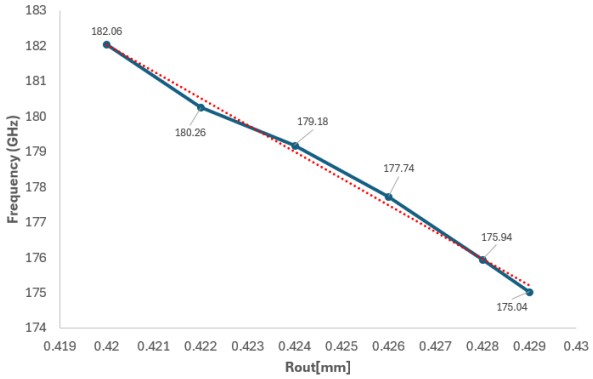

Figure 11.-. Tendence of the frequency displacement versus the radius increase where the dashed line represents the trend.

Table 3.- Results of the case 3

r_{out} [mm]	r_{in} [mm]	w [mm]	f_r [GHz]	S21 [dB]	Δf [GHz]	ΔS21 [dB]	Área [mm^2]	ΔÁrea [mm^2]
0.42	0.22	0.2	182.06	−47.63			0.805	
0.422	0.222	0.2	180.26	−47.49	1.8	−0.14	0.81	0.005
0.424	0.224	0.2	179.18	−49.04	1.08	1.55	0.815	0.005
0.426	0.226	0.2	177.74	−48.35	1.44	−0.69	0.82	0.005
0.428	0.228	0.2	175.94	−48.65	1.8	0.3	0.825	0.005
0.429	0.229	0.2	175.04	−49.2	0.9	0.55	0.827	0.0025

IV. CONCLUSIONS

The results of this work indicate that controlling the area of the resonators could be used to create a model that accurately describes the operating frequency based on the geometry of the resonator in the FSSs. Where obtained statistical values through analysis suggesting that the frequency displacement could double per area unit (see Table 4).

Table 4.- Statistical values

ΔÁrea [mm^3]	$\overline{\Delta f}$
0.0025	1.026
0.005	2.25
0.025	8.532
0.05	15.435

ACKNOWLEDGMENTS

The authors thank the Secretariat of Research and Postgraduate Studies of the National Polytechnic Institute for their support through projects SIP-20250096 and 20250035.

REFERENCES

[1] C. Zeng *et al.*, "Graphene-empowered dynamic metasurfaces and metadevices," *Opto-Electronic Advances*, vol. 5, no. 4, 2022, doi: 10.29026/oea .2022.200098.

[2] S. Nie and I. F. Akyildiz, "Metasurfaces for multiplexed communication," *Nat Electron*, vol. 4, no. 3, pp. 177–178, Mar. 2021, doi: 10.1038/s41928-021-00555-3.

[3] Y. Cheng, J. Liu, F. Chen, H. Luo, and X. Li, "Optically switchable broadband metasurface absorber based on square ring shaped photoconductive silicon for terahertz waves," *Physics Letters, Section A: General, Atomic and Solid State Physics*, vol. 402, Jun. 2021, doi: 10.1016/j.physleta.2021.127345.

[4] A. Maleki *et al.*, "Metamaterial-based octave-wide terahertz bandpass filters," *Photonics Res*, vol. 11, no. 4, p. 526, Apr. 2023, doi: 10.1364/prj.472109.

[5] T. Lang, J. H. Zhang, Y. Qiu, Z. Hong, and J. Liu, "Flexible terahertz Metamaterial sensor for sensitive detection of imidacloprid," *Opt Commun*, vol. 537, Jun. 2023, doi: 10.1016/j.optcom.2023.129430.

[6] C. M. Watts, X. Liu, and W. J. Padilla, "Metamaterial electromagnetic wave absorbers," *Advanced Materials*, vol. 24, no. 23, Jun. 2012, doi: 10.1002/adma.201200674.

[7] F. Chen, Y. Cheng, and H. Luo, "A broadband tunable terahertz metamaterial absorber based on single-layer complementary gammadion-shaped graphene," *Materials*, vol. 13, no. 4, Feb. 2020, doi: 10.3390/ma13040860.

[8] A. C. Tasolamprou *et al.*, "Experimental Demonstration of Ultrafast THz Modulation in a Graphene-Based Thin Film Absorber through Negative Photoinduced Conductivity," *ACS Photonics*, vol. 6, no. 3, pp. 720–727, Mar. 2019, doi: 10.1021/acsphotonics.8b01595.

[9] S. F. Shi *et al.*, "Controlling graphene ultrafast hot carrier response from metal-like to semiconductor-like by electrostatic gating," *Nano Lett*, vol. 14, no. 3, pp. 1578–1582, Mar. 2014, doi: 10.1021/nl404826r.

[10] M. Khazaei, A. Ranjbar, M. Arai, T. Sasaki, and S. Yunoki, "Electronic properties and applications of MXenes: a theoretical review," 2017, *Royal Society of Chemistry*. doi: 10.1039/c7tc00140a.

[11] B. Anasori and M. Naguib, "Two-dimensional MXenes," Mar. 01, 2023, *Springer Nature*. doi: 10.1557/s43577-023-00500-z.

[12] A. Iqbal, P. Sambyal, and C. M. Koo, "2D MXenes for Electromagnetic Shielding: A Review," Nov. 01, 2020, *Wiley-VCH Verlag*. doi: 10.1002/adfm.202000883.

[13] A. S. Solntsev, G. S. Agarwal, and Y. Y. Kivshar, "Metasurfaces for quantum photonics," May 01, 2021, *Nature Research*. doi: 10.1038/s41566-021-00793-z.

[14] Jitendra. Mohan and Abhinav. Gupta, *2019 International Conference on Signal Processing and Communication (ICSC) : 07-09 March 2019, Jaypee Institute of Information Technology, NOIDA*. IEEE, 2019.

[15] X. Chen, J. Tan, L. Kang, F. Tang, M. Zhao, and N. Kato, "Frequency Selective Surface Toward 6G Communication Systems: A Contemporary Survey," *IEEE Communications Surveys and Tutorials*, vol. 26, no. 3, pp. 1635–1675, 2024, doi: 10.1109/COMST.2024.3369250.

[16] S. Zahra *et al.*, "Electromagnetic Metasurfaces and Reconfigurable Metasurfaces: A Review," Jan. 14, 2021, *Frontiers Media SA*. doi: 10.3389/fphy.2020.593411.

[17] A. Ali, A. Mitra, and B. Aïssa, "Metamaterials and Metasurfaces: A Review from the Perspectives of Materials, Mechanisms and Advanced Metadevices," Mar. 01, 2022, *MDPI*. doi: 10.3390/nano12061027.

[18] M. Rittenhouse, F. Hopkinson, and D. Rittenhouse, "An Optical Problem, Proposed by Mr. Hopkinson, and Solved by Mr. Rittenhouse," 1786. [Online]. Available: https://www.jstor.org/stable/1005186

[19] R. K. Jaiswal, N. Pandit, and N. P. Pathak, "Metamaterial-FSS for THz Applications," 2022, pp. 1–23. doi: 10.1007/978-981-15-8597-5_24-1.

[20] F. Costa, A. Monorchio, and G. Manara, "Effi cient Analysis of Frequency-Selective Surfaces by a Simple Equivalent-Circuit Model," 2012.

[21] "Techniques for Analyzing Frequency Selective Surfaces-A Review."

[22] B. A. Munk and J. Wiley, "FREQUENCY SELECTIVE SURFACES Theory and Design A Wiley-Interscience Publication."

[23] S. Celozzi, R. Araneo, and G. Lovat, "Frequency Selective Surfaces," in *Electromagnetic Shielding*, Wiley, 2008, pp. 219–240. doi: 10.1002/9780470268483.ch10.

[24] S. Narayan, B. S. Rakesh, and M. Jha, "SPRINGER BRIEFS IN ELECTRICAL AND COMPUTER ENGINEERING COMPUTATIONAL ELECTROMAGNETICS Frequency Selective Surfaces based High Performance Microstrip Antenna." [Online]. Available: http://www.springer.com/series/13885

[25] X. Chen, J. Tan, L. Kang, F. Tang, M. Zhao, and N. Kato, "Frequency Selective Surface Toward 6G Communication Systems: A Contemporary Survey," *IEEE Communications Surveys and Tutorials*, vol. 26, no. 3, pp. 1635–1675, 2024, doi: 10.1109/COMST.2024.3369250.

[26] R. Alghamdi *et al.*, "Intelligent Surfaces for 6G Wireless Networks: A Survey of Optimization and Performance Analysis Techniques," *IEEE Access*, vol. 8, pp. 202795–202818, 2020, doi: 10.1109/ACCESS.2020.3031959.

[27] J. Ruan, Z. Meng, R. Zou, F. Cai, and S. Pan, "Miniaturized Frequency Selective Surface for 6G Communication," *Micromachines (Basel)*, vol. 13, no. 3, Mar. 2022, doi: 10.3390/mi13030427.

[28] K. Sarabandi and N. Behdad, "A frequency selective surface with miniaturized elements," *IEEE Trans Antennas Propag*, vol. 55, no. 5, pp. 1239–1245, May 2007, doi: 10.1109/TAP.2007.895567.

[29] M. Alberto, R. Barrera, W. Pereira Carpes, I. Del, and A. Resumen, "Visión Electrónica4728 • bOgOTá (cOLOmbIA) VISIÓN INVESTIGADORA," vol. 12, no. 2, 2018, doi: 10.14483/22484728.14267.